Max-Planck-Institut
für Meteorologie

REPORT No. 97

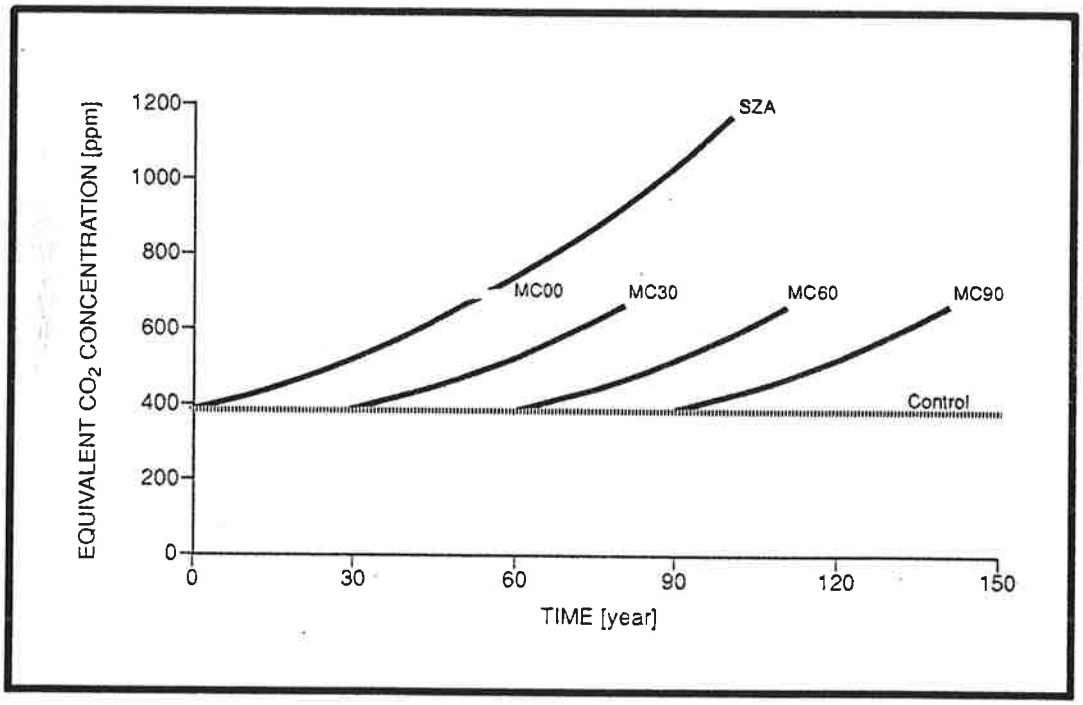

MONTE CARLO CLIMATE CHANGE FORECASTS WITH A GLOBAL COUPLED OCEAN–ATMOSPHERE MODEL

by

U. CUBASCH • B. D. SANTER • A. HELLBACH • G. HEGERL • H. HÖCK
E. MAIER-REIMER • U. MIKOLAJEWICZ • A. STÖSSEL R. VOSS

HAMBURG, DECEMBER 1992

AUTHORS:

G. Hegerl
H. Höck
E. Maier–Reimer
U. Mikolajewicz
A. Stössel

Max–Planck–Institut
für Meteorologie

R. Voss

Universität Hamburg
Meteorologisches Institut
Bundesstraße 55
D–2000 Hamburg 13
FRG

U. Cubasch
A. Hellbach

Deutsches Klimarechenzentrum (DKRZ)
Bundesstraße 55
D–2000 Hamburg 13
FRG

B. D. Santer

Program for Climate Model Diagnosis
and Intercomparison
Lawrence Livermore National Laboratory
Livermore
California 94550
USA

MAX–PLANCK–INSTITUT
FÜR METEOROLOGIE
BUNDESSTRASSE 55
D–2000 HAMBURG 13
F.R. GERMANY

Tel.: +49 (40) 4 11 73–0
Telex: 211092 mpime d
Telemail: MPI.METEOROLOGY
Telefax: +49 (40) 4 11 73–298

ISSN 0937–1060

Monte Carlo Climate Change Forecasts with a Global Coupled Ocean-Atmosphere Model

U. Cubasch[1], B. D. Santer[2], A. Hellbach[1], G. Hegerl[3], H. Höck[3], E. Maier-Reimer[3], U. Mikolajewicz[3], A. Stössel[3] and R. Voss[4]

1: Deutsches Klimarechenzentrum, Bundesstr. 55, D-2000 Hamburg 13, FRG

2: Program for Climate Model Diagnosis and Intercomparison/Lawrence Livermore National Laboratory, Livermore, Ca. 94550, USA

3: Max-Planck-Institut für Meteorologie, Bundesstr. 55, D-2000 Hamburg 13, FRG

4: Meteorologisches Institut der Universität Hamburg, Bundesstr. 55, D-2000 Hamburg 13, FRG

correspondence to: U. Cubasch

Abstract

The Monte Carlo approach, which has increasingly been used during the last decade in the field of extended range weather forecasting, has been applied for climate change experiments. Four integrations with a global coupled ocean-atmosphere model have been started from different initial conditions, but with the same greenhouse gas forcing according to the IPCC scenario A. All experiments have been run for a period of 50 years.

The results indicate that the time evolution of the global mean warming depends strongly on the initial state of the climate system. It can vary between 6 and 31 years. The Monte Carlo approach delivers information about both the mean response and the statistical significance of the response. While the individual members of the ensemble show a considerable variation in the climate change pattern of temperature after 50 years, the ensemble mean climate change pattern closely resembles the pattern obtained in a 100 year integration

and is, at least over most of the land areas, statistically significant. The ensemble averaged sea-level change due to thermal expansion is significant in the global mean and locally over wide regions of the Pacific.

The hydrological cycle is also significantly enhanced in the global mean, but locally the changes in precipitation and soil moisture are masked by the variability of the experiments.

1.0 Introduction

The impact of the emission of anthropogenic greenhouse gases on the climate can be simulated reliably only with a coupled global ocean-atmosphere model (Houghton et al, 1990). The enormous amount of computer resources required for these experiments, however, has limited the number of institutions which have actually performed such integrations to only four. These institutions could up to now afford to run only one single climate change simulation, so that currently there exist in the literature only four extended climate change integrations with coupled ocean-atmosphere models. Each integration makes different assumptions about the future increase of the greenhouse gases, and the individual models have different sensitivities and different spatial resolutions (Houghton et al, 1992).

On the 100 year time-scale, it is likely that the variability of the ocean dominates the climate system. If the ocean surface exhibits cooling due to natural variability alone, a greenhouse warming signal might be masked, thus increasing the time that it would take in order to discriminate between the signal and the background noise. On the other hand, if the ocean has a warming trend, it might exaggerate the greenhouse warming signal. The problem of defining a greenhouse signal relative to the natural variability of the coupled ocean-atmosphere system is compounded by the fact that comprehensive 4-dimensional data sets of the observed state of the ocean circulation are not available. All coupled model simulations therefore start with an ocean which has been spun up for hundreds to thousands of years in order to accurately represent present day mean conditions. However, it is virtually impossible to determine wether the sub-surface initial conditions in the ocean model coincide with the present 'observed' state of the ocean. A single simulation, there-

fore may be unrepresentative of the "true" space-time greenhouse signal, since the current trend within the ocean model caused by long-term variability might not coincide with the trends in the real ocean. Additionally, even in the atmosphere on its own, circulation anomalies can persist for decades. They are caused by nonlinear interactions within the atmosphere (Hansen et al, 1988; Lorenz, 1991). A single climate change integration is therefore not representative for all possible states the climate system can adopt in the time-scale considered here and does not allow any statement on the statistical significance of the prediction.

Furthermore, studies of the individual integrations have shown that the large internal variability of the modelled (and the natural) climate system makes it difficult to detect the climate change signal (Meehl et al, 1992; Manabe et al, 1992; Santer et al, 1992).

In the present study, four climate change simulations have been carried out with the same model. However, each simulation started at different times of the control simulation. All other parameters, including the change of the radiative forcing according to the IPCC scenario A (Houghton et al, 1990), remain the same. This approach, known as the "Monte Carlo Method" in numerical weather prediction, gives a prediction about a future change and yields an estimate of the confidence limits of the forecasts.

Firstly, the technical details of the "Monte Carlo" Method will be described (chapter 2). In the next section (chapter 3) the results and the sensitivity of the results to the precise definition of the climate change will be discussed.

2.0 The Experiment

2.1 The Model

The coupled global ocean-atmosphere model used in this experiment has been described in Cubasch et al (1992). The atmospheric component comprises 19 levels in the vertical and a horizontal resolution of T21 (with a Gaussian grid of 5.625 ^{o}). It has been coupled synchronously to the LSG Ocean model with a horizontal grid spacing similar to the Gaussian grid of the T21 model and 11 layers in the vertical. This model has been used in a number of climate change experiments (Bakan et al, 1991; Cubasch et al, 1992). The control and the scenario A simulation described in the latter paper form the basis for the experiments introduced here.

2.2 The Monte Carlo Method

As pointed out in the introduction, the presence of variability on the timescale of the predicted phenomenon makes it necessary to assess its impact on the predicted signal. In the present paper this is done using the "Monte Carlo" (MC) Method: Several identical climate change experiments are run from different initial conditions. A similar method, which originally has been applied in extended range forecasting experiments (Molteni et al, 1988; Brankovic et al, 1990) has already been employed for climate change studies by Hansen et al (1988) to investigate the long-term variability in their integration. The 100 year control simulation with a coupled ocean-atmosphere model described in Cubasch et al (1992) has been used to provide initial conditions for the MC experiments. As can be seen in the schematic diagram (Fig. 1), the experiments have been started at 30 years intervals with initial fields of the control experiment at years 0, 30, 60 and 90 with the radiative forcing of the IPCC (1990) scenario A starting in the year 1985. They are referred to in the text as MC00, MC30, MC60 and MC90. All simulations have been run with the same coupled global ocean-atmosphere model described in Cubasch et al (1992) for 50 years. The

first MC experiment (MC00) is identical to the first 50 years of the 100 year Scenario A experiment described in Cubasch et al (1992), here referred to as SZA.

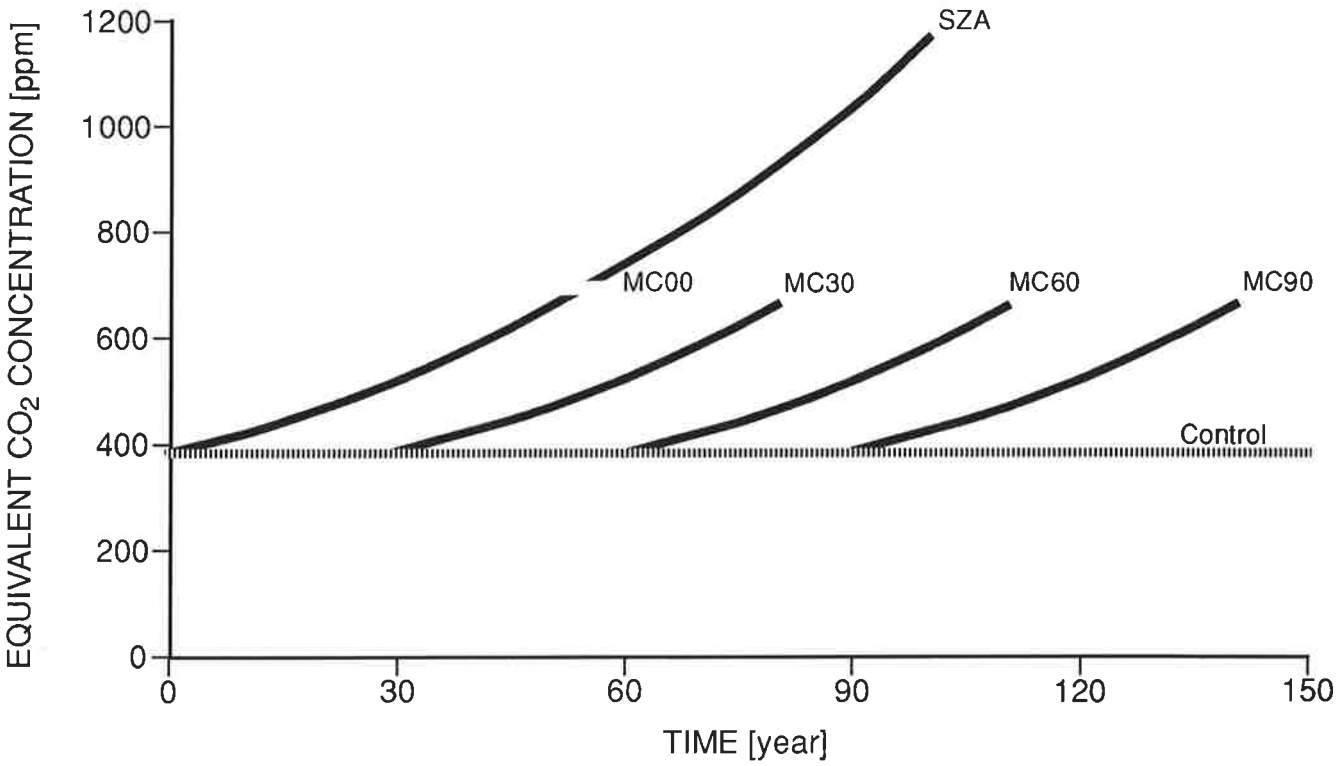

Figure 1. Schematic diagram of the "Monte Carlo" climate forecasts.

3.0 Results

3.1 Global Mean Temperature Rise

The temperature of the climate change experiment can be represented by the sum of following terms:

$$T = T_0 + T_\alpha + T_f + T'$$

with

T_0: the initial temperature

T_α: temperature drift

T_f: externally forced temperature

T': internal temperature variability

A change in the temperature can therefore be caused by drift, by the external forcing or internal fluctuations:

$$\Delta T = T_{\text{climate change}} - T_{\text{control}} = (T_0 + T_\alpha + T_f + T')_{\text{climate change}} - (T_0 + T_\alpha + T')_{\text{control}}$$

All calculations have been done with

$$(T_0)_{\text{climate change}} = (T_0)_{\text{control}}$$

and under the assumption that

$$(T')_{\text{climate change}} = (T')_{\text{control}}$$

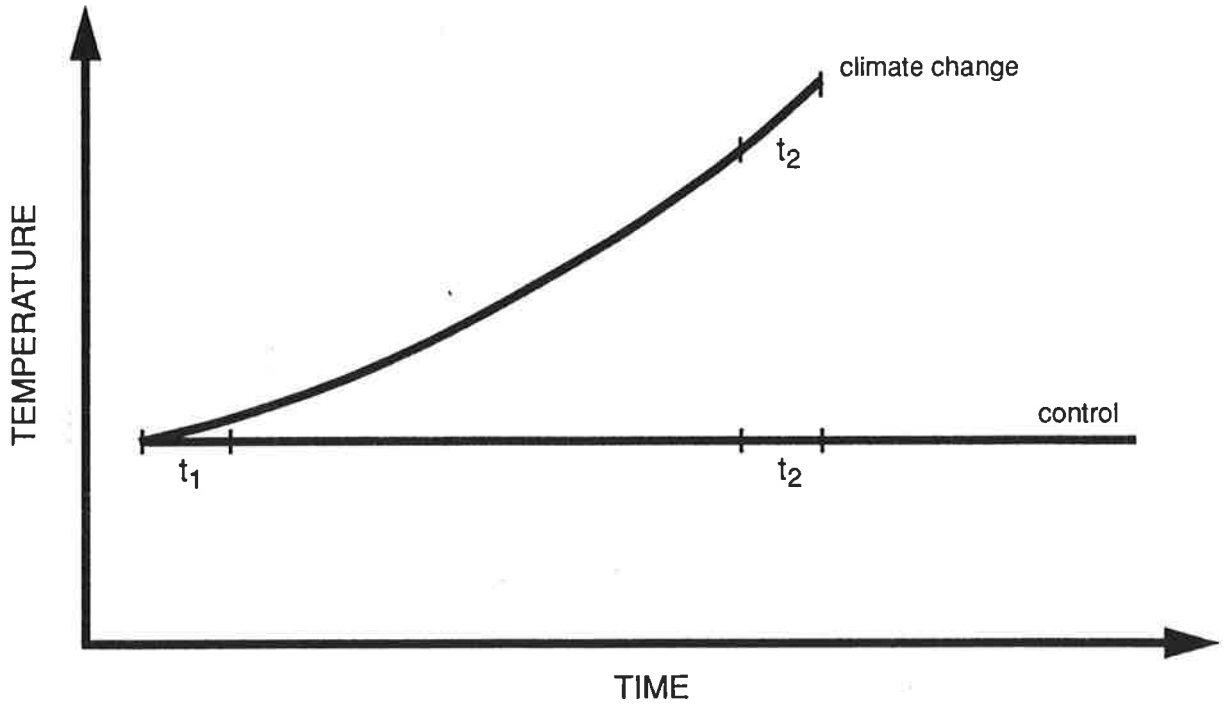

Figure 2. Schematic diagram of possible ways to calculate a climate change.

For the calculation of the changes of most of the parameters Definition 1 in accordance with Cubasch et al (1992) has been used and extended to the MC simulations: The anomaly of each experiment is defined as the difference of the climate change experiment to the 10 years of the control experiment beginning at the start of the climate change simulation (Fig. 2):

$$\Delta T_{Def\ 1} = T_{climate\ change}\ (t2) - T_{control}\ (t1)$$

The ensemble mean has been calculated accordingly as the mean of the anomalies generated in the above defined fashion. This definition assumes that changes in the control simulation are caused only by relatively short-term natural variability and that no drift exists

(i.e. $T_\alpha = 0$). To clarify some of the results obtained by usage of Definition 1, Definition 2 has been applied as well. In Definition 2 the same years of the control experiment are subtracted from the same year of the climate change experiment:

$$\Delta T_{Def\ 2} = T_{\text{climate change}}(t2) - T_{\text{control}}(t2)$$

Definition 2 is correct under the assumption that both climate change and control experiment exhibit the same climate drift or very long-term climate variability:

$$((T_\alpha)_{\text{climate change}} = (T_\alpha)_{\text{control}}).$$

The final choice of either definition is somewhat arbitrarily, because both assumptions are normally not completely fulfilled (Santer et al, 1992). In this paper Definition 1 has been used as the preferred definition to facilitate comparison of results with Cubasch et al (1992). However, for the sea level change and the change in sea ice, Definition 2 appeared more appropriate due to the obvious long periodic variability in these quantities (c. f. Fig. 15 a).

As it has been pointed out in Cubasch et al (1992), the annually averaged global mean near surface atmospheric temperature of the control simulation fluctuates with a maximum anomaly of - 0.4 K during the 100 year of integration time (Fig. 3a). There is a distinct drop in the global mean temperature between year 50 and 70 of -0.3 K. Due to the short length of the integration it is not clear whether this drop is a reflection of a real long term variability or some residual climate drift, which might be caused by inconsistencies in the coupling of the model components and might be related to the problems in the simulation of the sea ice. Two of the MC integrations start before, two after this temperature drop.

All MC simulations display only a small warming at the beginning of the integration. This phenomenon is apparently caused by the experimental procedure which neglects the effect of prior oceanic warming from the early days of industrialization up to 1985. This "cold-

start" has been discussed in Hasselmann et al (1992) and Fichefet and Tricot (1992). The latter estimated the temperature error due to the cold start to be as large as 30% of the warming signal after 50 years of integration time (at the year 2035), when the experiment is started at 1985 conditions instead of pre-industrial conditions. Even without the consideration of the cold start problem, the IPCC curve for scenario A lies just outside the upper 95% bracket (2 *σ) generated by the four MC experiments (Fig.3b). The lower 95% bracket includes a period of no appreciable temperature rise for more than 30 years.

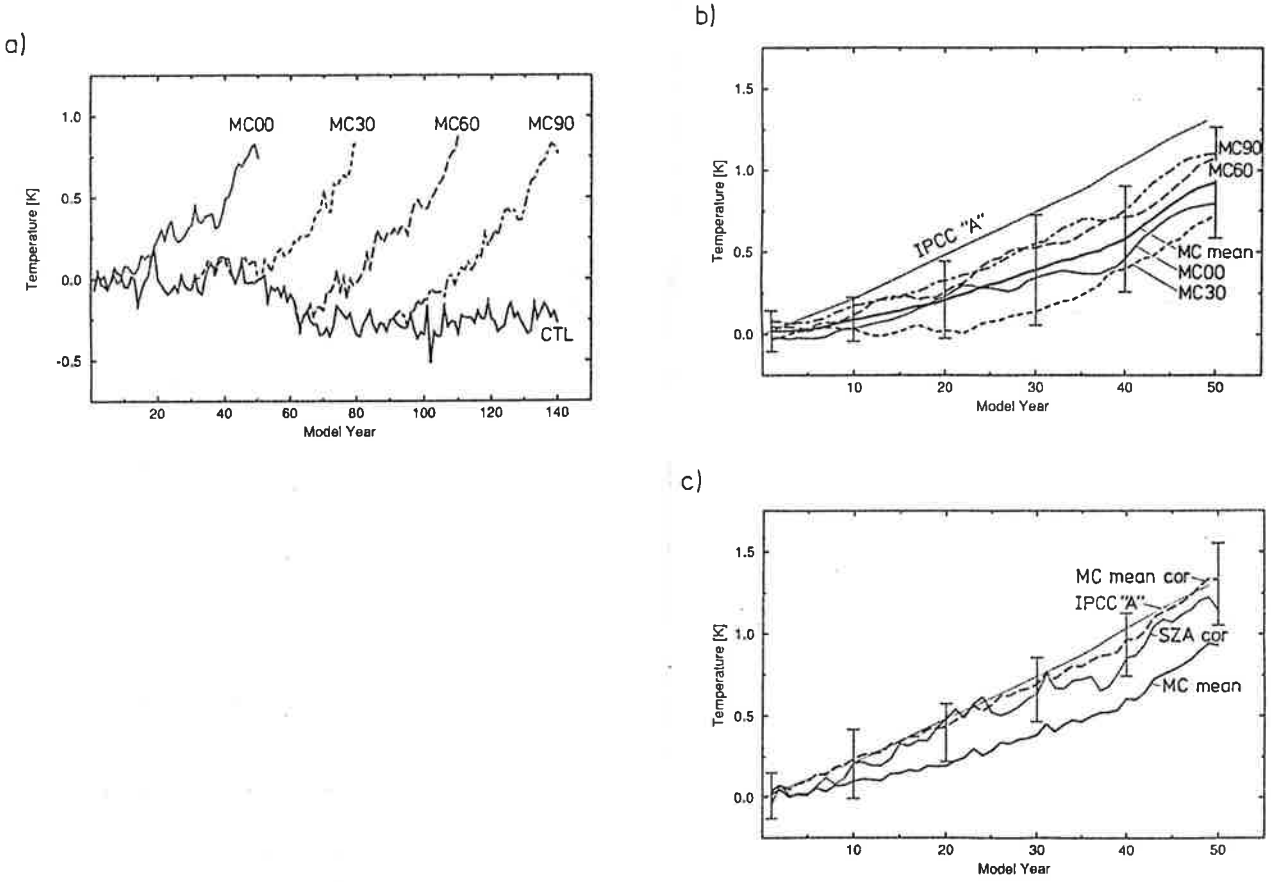

Figure 3. The time evolution of the global mean surface temperature change (^{o}C) for the four "Monte-Carlo" Simulations and the control experiment (a); the time evolution of the global mean surface temperature change (^{o}C) for the four "Monte-Carlo" simulations (smoothed), the mean over all four simulations (smoothed), the 95% significance limit and the IPCC "best estimate" after Houghton et al (1990) (b); and the time evolution of the cold start corrected global mean surface temperature change in the mean over all MC integrations (smoothed), the 95% significance limit, the cold start corrected curve for a 100 year scenario A calculation after Cubasch et al (1992) and the IPCC "best estimate" (c).

The "cold start" problem was investigated by Hasselmann et al (1992) for the SZA experiments. In this report the warming delay by the "cold start" is estimated by a linear response model. An exponential function, which forms the basis to the response model, has been fitted for the individual MC integrations as well as for the ensemble mean (for further details see Hasselmann et al, 1992). Using this approximation, the cold start response function R(t) in a simulation is represented by the formula:

$$R(t) = \alpha/\mu \, (1 - e^{-\mu t})$$

where α describes the rate of temperature increase per year and μ the time constant.The characteristic constants are displayed in Table 1.

Experiment	warming after 50 years [K]	detection time [a]	μ = time-constant $[a^{-1}]$	α = rate of increase [K/a]	RMS of fit [K]	temperature error at t=infinity [K]
SZA	0.8	15.	1./37.	0.06	0.06	0.6
MC00	0.8	15.	1./83.	0.05	0.07	1.3
MC30	0.8	31.	1./373.	0.05	0.08	7.1
MC60	0.9	11.	1./77.	0.06	0.06	1.4
MC90	1.1	6.	1./8.	0.20	0.05	0.2
MC mean	0.9	16.	1./30.	0.07	0.03	0.5

Table 1: The start characteristics of the "Monte Carlo" climate simulations for the global mean near surface temperature.

Due to the large variability within the individual curves and the short length of the records, the fit of the exponential curves is not very stable. Therefore the coefficients α of the fitted

exponential functions differ widely varying from 0.05 K/a to 0.20 K/a. The characteristic response time $1/\mu$ varies between 8 and 373 years. The largest temperature rise in the whole ensemble is found in MC90. This is reflected in the shortest characteristic time of 8 years and an increase rate of 0.2 K/a in this experiment, while MC30, on the other hand, has an extremely long characteristic time of 373 years connected with a low rate of temperature rise (0.05 K/a).

The temperature of the MC ensemble rises by 0.07 K/a and has a characteristic time of 30 years. Due to the smooth appearance, the ensemble mean can be much better represented by an exponential function than the individual members of the ensemble. This is reflected in the low root mean square (RMS) error of the fit, which is only half as large for the ensemble mean as for the individual members.

The exponential function fitted to the ensemble mean has subsequently been used to estimate the cold start correction in a similar way to the method used by Hasselmann et al (1992). If the individual members of the ensemble are corrected for the cold start, some of the curves lie higher than the IPCC "best estimate", some of them below. Overall, the spread between the highest and the lowest realization for a single year can be as large as 0.3 K. Related to an average temperature rise of 0.03 K per year this spread can be interpreted as an uncertainty in the timing of an temperature change of about 10 years, depending on the state of the climate system.The ensemble mean temperature rise corrected for the cold start has a deviation smaller than 0.1 K from the IPCC "best estimate" (Fig. 3c). When all temperature increases produced by the individual members of the ensemble are corrected with the cold start correction of the ensemble mean, the error margin, which is defined by the $2 * \sigma$-limits around the ensemble mean, reaches +/- 0.3 K and is almost independent of the time elapsed since the start of the climate change experiments.

It is interesting to note that the 100 year scenario A experiment analysed by Hasselmann et al (1992) is, by chance, quite a good proxy for the cold start behavior of the ensemble

average. The curve for the cold start corrected MC average lies slightly higher than the one of the 100 year scenario A experiment and is therefore closer to the IPCC "best estimate".

A simple measure of the detection time t_d can be defined as the time when the CO_2 warming signal exceeds the mean of the control experiment by two standard deviations (assuming that the drift T_α is negligable):

$$T_f > T_0 +/- 2 * \sigma$$

This detection time t_d can be as short as 6 years or as large as 31 years (c. f. Table 1). It reflects therefore not only the problems in the experimental procedure, the so called "cold start", which should be independent of the initial state of the climate system, but also indicates the importance of the state of the ocean at the start of the integration.The average value is 16 years.

To determine the major influences on the detection times, we investigated a number of variables, which, for physical reasons, could be responsible for a difference in the rate of warming of the modeled system (the wind stress, the vertical convection and the ice coverage). There is some indication that the detection time is correlated with the ice thickness and with the cloud cover in the Arctic. However, this correlation appears to be related to the drift in ice thickness, which did not stabilize before year 60 of the control simulation (Cubasch et al, 1992). No clear signal could be identified in any other quantity, probably due to the small sample size.

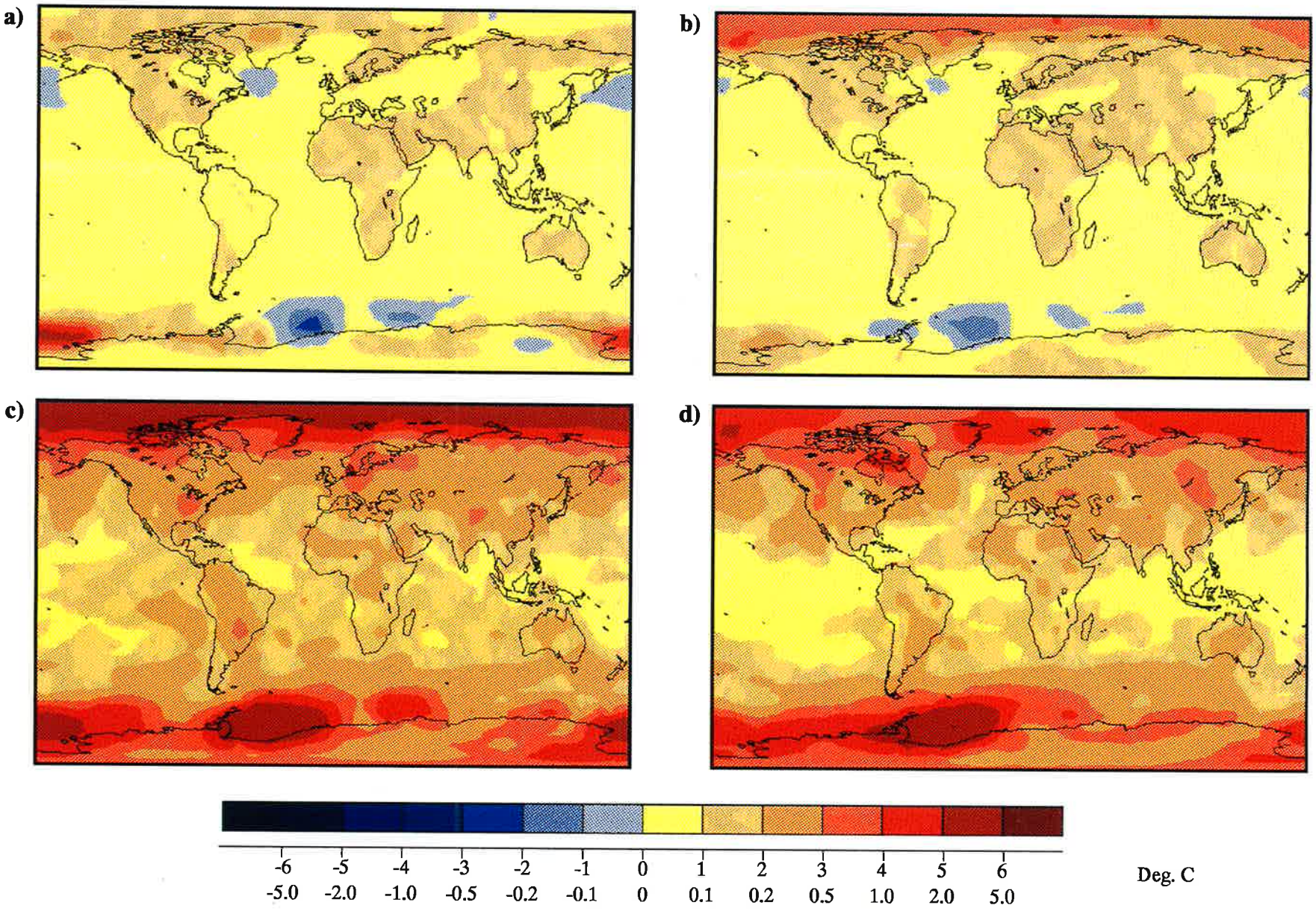

Figure 4. The distribution of the change in annually and ensemble averaged near surface temperature for the final decade of the MC integrations (Definition 1: a, Definition 2: b), and the standard deviation of the temperature change of the members of the ensemble to the mean (Definition 1: c, Definition 2: d).

3.2 Regional Changes

3.2.1 2 m Temperature

The regional distribution of the temperature rise for the last 10 years of the MC ensemble after Definition 1 (Fig. 4a) shows a comparatively stable climate change pattern over the land areas in the tropics and the mid-latitudes which resembles the 2m temperature change pattern of the scenario A experiment described in Cubasch et al (1992), but with reduced amplitude. It is interesting to note that even the regions of cooling in the North Atlantic and North Pacific are a stable feature in all integrations and are clearly visible in the mean over all MC simulations. In these regions the standard deviation between the experiments is small (Fig. 4b). The maximum standard deviation between the integrations is reached at high latitudes of the Northern and Southern Hemisphere, particularly in the Arctic and Antarctic regions, where it is as large as the climate change signal. The MC experiment starting at year 30 (MC30) shows an extensive cooling in the Arctic, while the MC experiments starting at year 60 (MC60) and 90 (MC90) show an extensive warming in this area (Fig. 5).

The reasons for this different behavior in the Arctic can partially be explained by the changes in the ice volume during the first part of the control integration (see section 3.2.3). During a global warming in the northern hemisphere the ice thickness decreases, which results in a temperature increase due to the larger heat flux through the ice (Manabe et al, 1992). As we employ Definition 1, i. e. the first years of the control experiments are subtracted from the last 10 years of the climate change experiment, the ice thickness for the first two MC experiments becomes larger than their respective starting value (see Fig. 10a), which ultimately results in the cooling relative to the starting value. If the climate change over ice covered regions is calculated according to Definition 2, this cooling is replaced by a slight warming (Fig. 6).

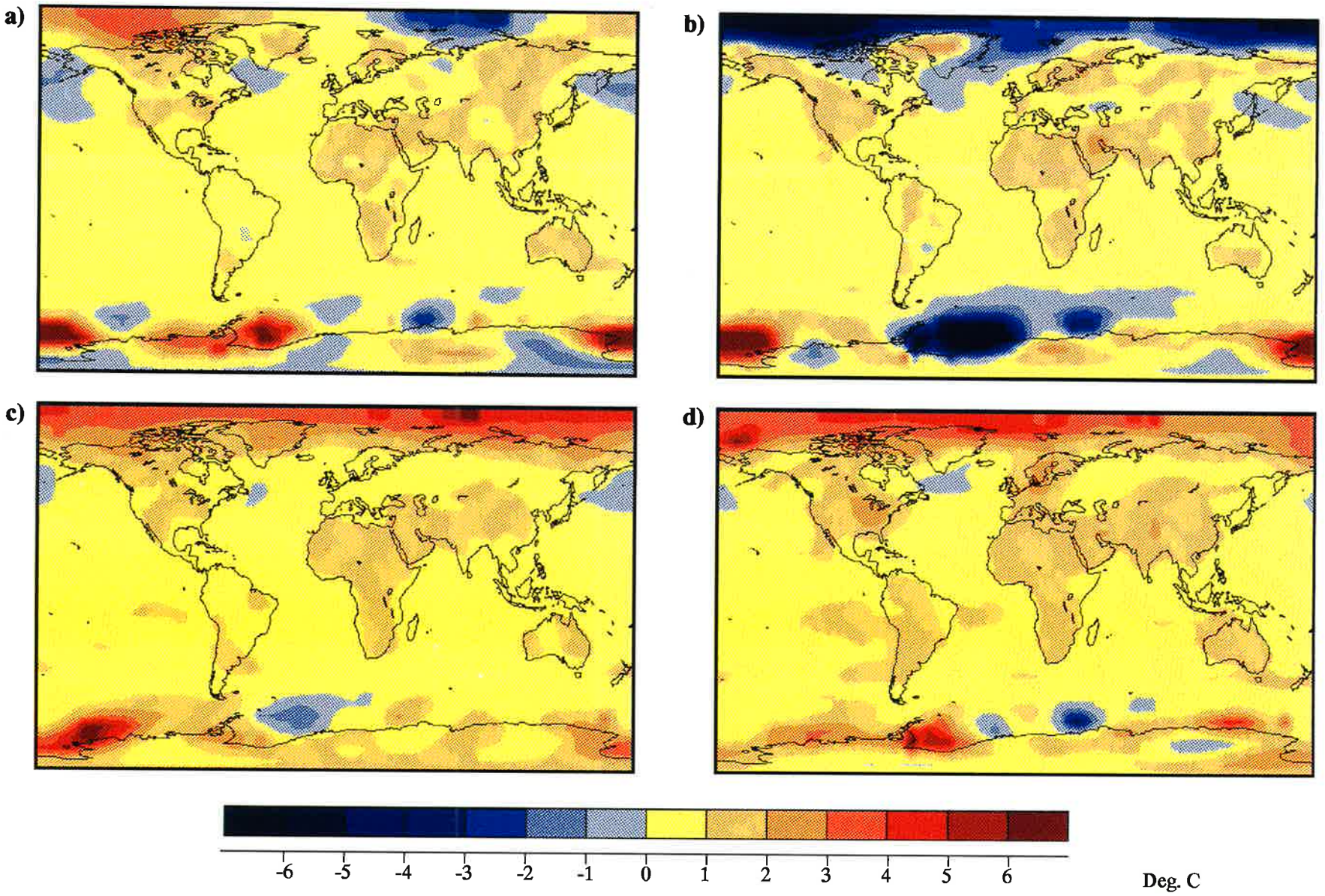

Figure 5. The distribution of the change in annually-averaged near surface temperature for the final decade of the MC integrations after Definition 1. a): MC00, b): MC30; c): MC60 and d): MC90.

Using this definition, the corresponding ice thickness of the control experiment is larger than in the individual MC experiments, even for the first two experiments, because the drift in the ice thickness is taken into account.

In the Antarctic the differences in warming and cooling between the experiments are mainly related to changes in the ice-coverage in the Ross- and Weddell Sea. The extensive cooling areas emerging in the MC30 experiment in the Weddell sea are due to a warming in the control experiment, which is connected with a sudden decrease of the ice coverage in the Weddell sea (Fig. 10 d).

When a univariate t-test is applied locally, the warming over most of the continents with the exception of a large region stretching from Greece to central Russia is significant at the 95% level. Therefore, the warming of the landmasses is a stable climate change feature. Over sea, only the central Pacific shows a significant warming.

As the space points are not statistically independent, additionally an multivariate pattern test has been performed in order to reject the null-hypothesis of no significant warming. We calculated the vector-product of a spatial guess pattern of the expected global warming with the output of our integrations for this test. Two different guess patterns have been derived from the smoothed output of the scenario A and the "2xCO_2" experiment mentioned in Cubasch et al. (1992). Samples of decadal means of the control run were used to define the statistical properties of the resulting univariate random variable. The vector-product of the temporal means of the last decade of the four MC integrations with the guess pattern exceeds the standard deviation by a factor of around eight for both cases. Hence the warming of the MC runs is highly significant.

The regional distribution of the temperature change (Definition 1) in the MC experiments also varies considerably with the seasons. The Antarctic experiences a cooling in local summer (DJF). This cooling is a stable feature in all integrations. In the same season the

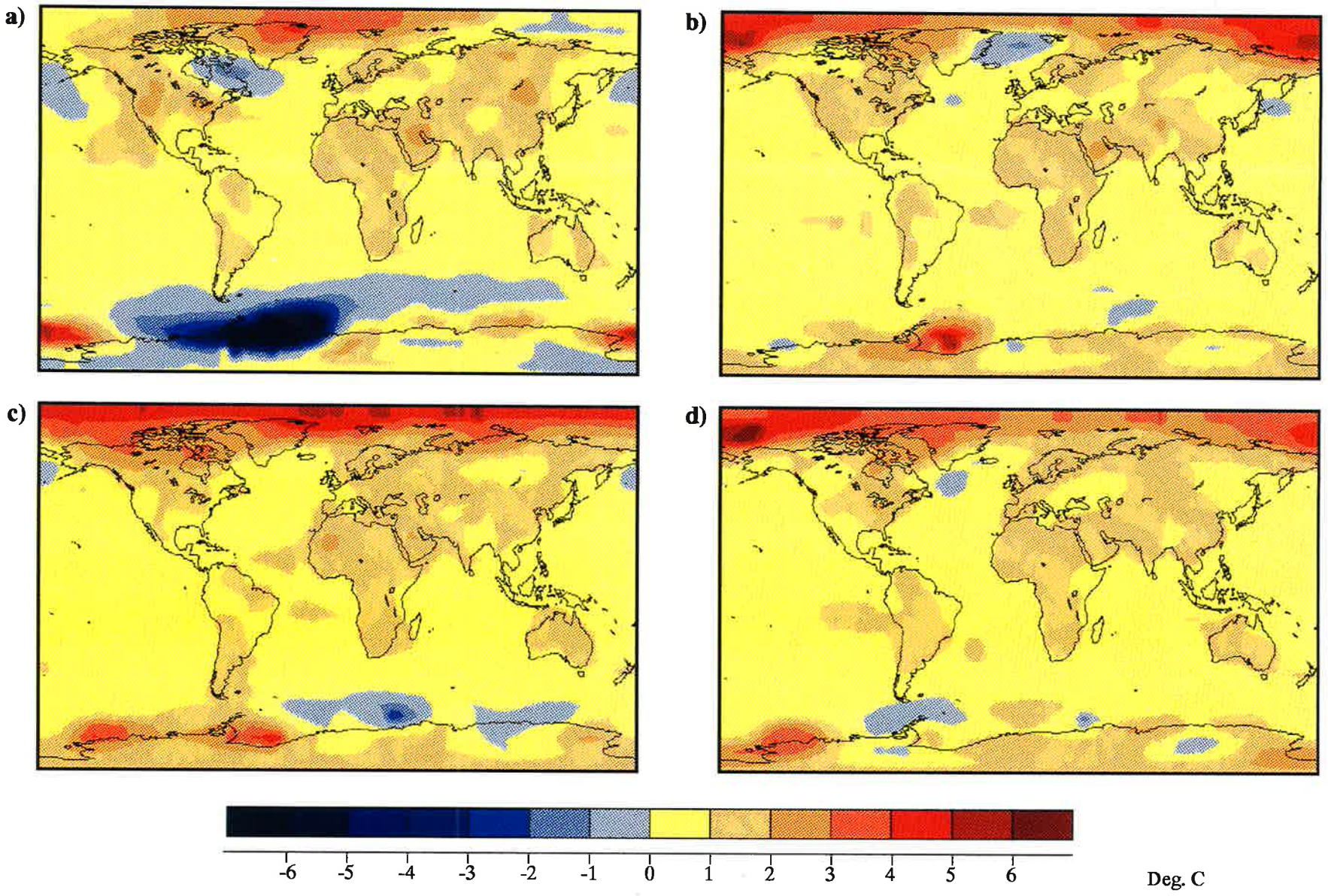

Figure 6. The distribution of the change in annually-averaged near surface temperature for the final decade of the MC integrations for Definition 2. a): MC00, b): MC30; c): MC60 and d): MC90.

Arctic experiences a warming. This warming is, as in case of the annual mean, influenced by the drift in the ice thickness. A cooling region situated near Greenland, which is related to a reduction of deep vertical mixing in the ocean, is simulated in all experiments. In southern winter (JJA) the Antarctic land mass warms up in all integrations. Near the ice edge, cooling takes place due to a reduced exchange with the water in the deeper ocean layers. Near the Ross Sea there is distinct warming emerges due to a reduced ice thickness. The MC30 experiment is the only integration in which the Ross sea cools. This is due to the large ice melting in the control experiment, a feature, which is not present in the climate change experiment as well. As in the annual mean, the largest variability between the experiments can be found in the high latitudes of both hemispheres. On the whole, the seasonal distribution of the climate change in the surface temperature is similar to that described in the IPCC report (1992).

3.2.2 EOF Analysis of 2m Temperature Changes

An EOF analysis of the near surface temperature of each member of the MC integration is performed for Definition 1 as well as for Definition2.

Independent of the definition, the first EOF (Fig. 7, 8) shows a large variability of the signal in the high latitudes of both hemispheres. In low and mid-latitudes the patterns in all MC integrations are generally spatially coherent and show a pronounced land-sea contrast component. The variability at high latitudes in both hemispheres is sometimes out of phase with variability in the tropics and mid-latitudes, particularly in the case of MC00 (Definition 1 and 2) and MC30 (Definition 2). Note also that in the case of the MC00 and MC30 experiments, the two signal definitions yield markedly different dominant EOF patterns.

If Definition 1 is applied, the total space-time variance explained by the EOF 1 pattern varies between 50% and 67%. This is lower than the variance explained by the dominant

pattern in the 100-year SZA integration (84%; see Cubasch et al. 1992), which is simply due to the shorter integration time of the MC simulations. Note that the first EOF of the ensemble mean response (Fig. 9a) explains more of the total space-time variance (78%) than any of the individual MC integrations. When Definition 2 is applied (Fig. 8), the first EOF in each of the MC simulations explains less variance than under Definition 1 (Table 2). This difference is due to the fact that Definition 2 superimposes the interannual variability of the control simulation upon the variability of the climate change experiment, whereas Definition 1 considers the interannual variability of the perturbation experiment only.

In order to make a more objective comparison between the EOF 1 patterns of the individual members of the ensemble of MC experiments, we computed area-weighted anomaly pattern correlations with and without subtraction of the spatial mean component (r and r^*, respectively; see Santer et al., 1992). For Definition 1, the between-integration pattern correlations (with spatial mean subtracted) do not exceed 0.31, mainly due to pattern differences at high latitudes (see Fig. 7 and Table 2). When the spatial mean is incorporated, the large-scale spatial coherence of the EOF 1 patterns in MC60 and MC90 substantially improves the pattern correlation ($r = 0.26$ vs. $r^* = 0.78$; see Table 3).

The EOF 1 patterns calculated under Definition 2 are generally more highly intercorrelated than under Definition1. This is true for both r and r^* (see Tables 2 and 3), and is due to the fact that the EOF 1 patterns computed under Definition 2 tend to have a more spatially-coherent structure at high latitudes, particularly in the Northern Hemisphere. The lower between-experiment pattern correlations under Definition1 are strongly dependent on the amplitude and spatial coherence of the decadal mean control patterns which are used to calculate the signal anomaly.

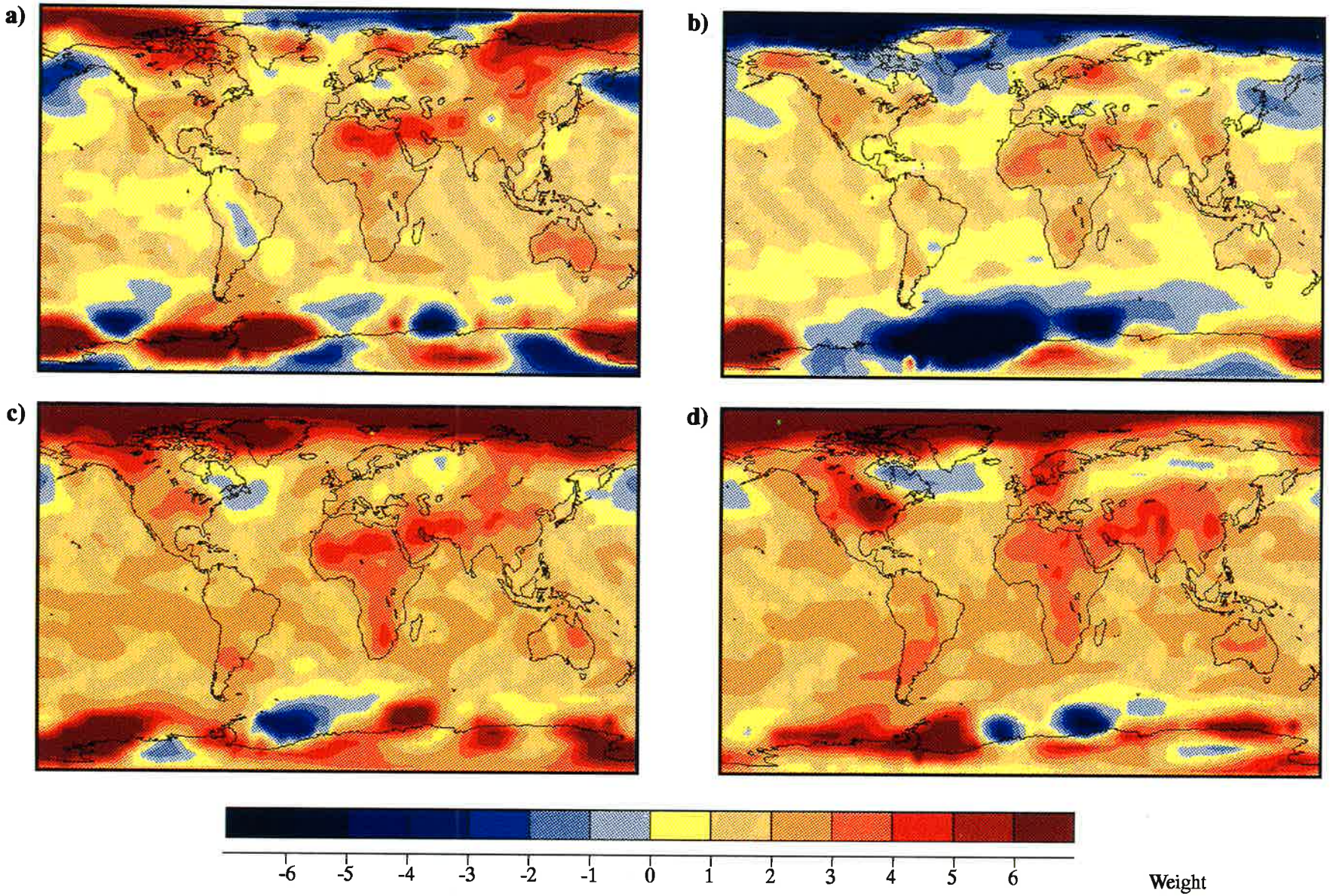

Figure 7. The first EOF [*10^2] of the near surface temperature change of the four members of the MC simulation for Definition 1. MC00 (a), MC30 (b), MC60 (c) and MC90 (d).

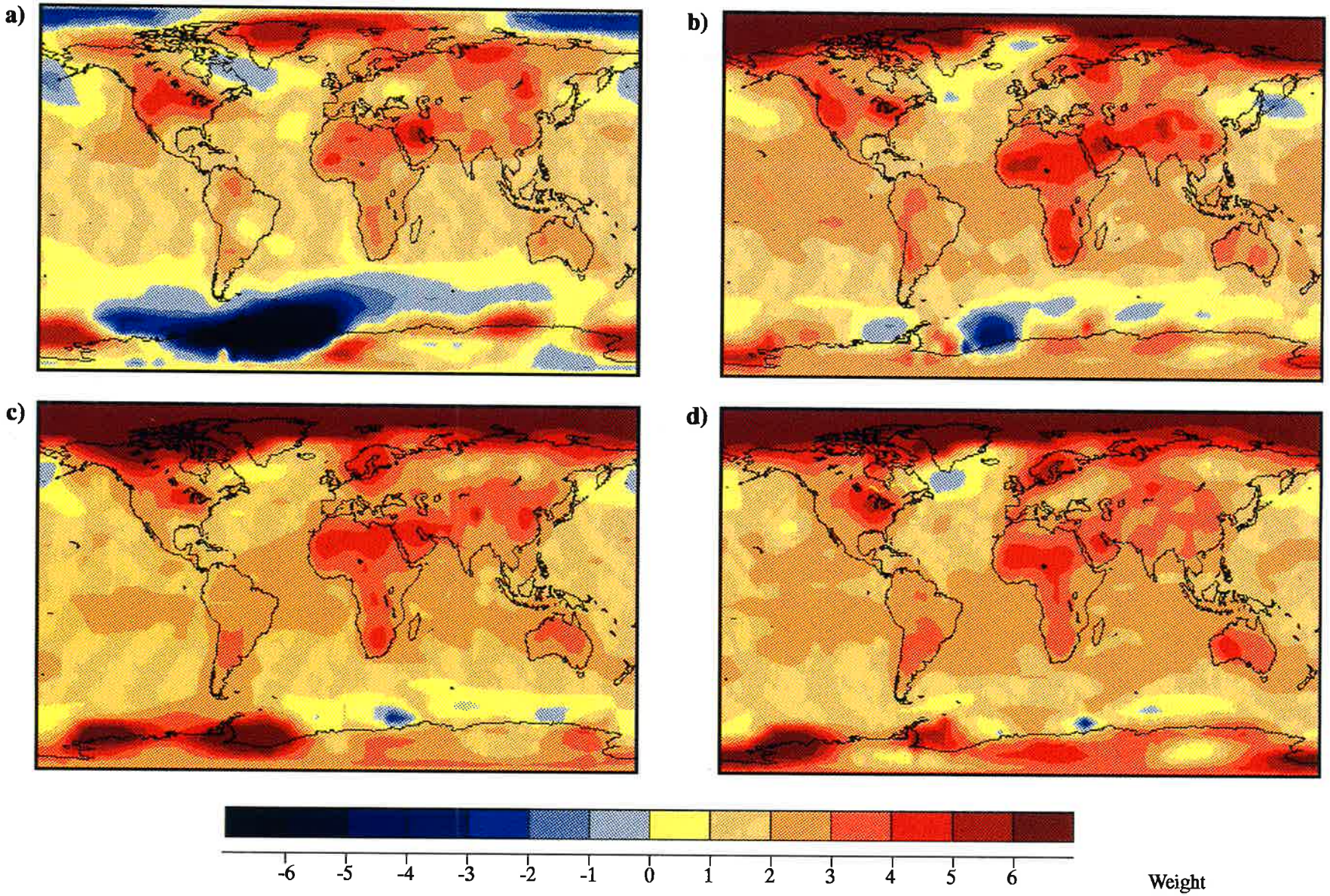

Figure 8. The first EOF [*10^2] of the near surface temperature change of the four members of the MC simulation for Definition 2. MC00 (a), MC30 (b), MC60 (c) and MC90 (d).

correlation between Def1 and Def2	MC00	MC30	MC60	MC90	MC mean	SZA	explained variance (Def 1)
MC00	**0.02**	0.06	0.20	0.26	0.54	0.76	0.50
MC30	*0.47*	**0.28**	0.31	0.07	0.76	0.47	0.67
MC60	*0.12*	*0.62*	**0.50**	0.26	0.61	0.53	0.56
MC90	*0.30*	*0.73*	*0.80*	**0.69**	0.51	0.44	0.62
MC mean	*0.80*	*0.83*	*0.65*	*0.77*	**0.75**	0.86	0.77
SZA	*0.66*	*0.85*	*0.64*	*0.80*	0.92	**0.56**	0.84
expl. var. (Def. 1)	*0.44*	*0.30*	*0.41*	*0.39*	*0.67*	*0.76*	

Table 2: Between-integration pattern correlations for EOF 1 of the individual members of the ensemble of MC experiments and the mean of the ensemble. All correlations are computed with removal of the spatial mean component (r). Results are for Definition 1 (upper triangle of matrix) and Definition 2 (lower triangle of matrix and italics) of the signal. The explained variance of the EOF 1 pattern under both definitions is also given. The diagonal elements of the matrix (bold) give the correlation of the EOF 1 pattern of the same experiment under the two definitions.

The first EOF for MC00 calculated under Definition2 (Fig. 8a) and the first EOF of MC30 calculated under Definition 1 (Fig. 7b) both display a very similar pattern in the southern ocean. This is caused by a large fluctuation in sea ice coverage in the Weddell Sea in the control experiment between years 30 to 60, resulting in strong warming of the Weddell Sea region in the control experiment. Under Definition 1 this anomaly pattern is projected onto the MC30 experiment (since the decadal average of years 31-40 of the control is subtracted), while under Defintion 2 it influence the signal in MC00 experiment. This anomalous behavior of the control run during years 30 to 60 explains why the correlation between the EOF 1 patterns generated under both definitions (the diagonal elements of Tables 2 and 3) is small for the MC00 and MC30 experiments, and large thereafter.

The pattern of the first EOF of the ensemble mean of the MC experiments closely resembles the pattern of the scenario A (SZA) experiment after 100 years ($r = 0.86$, $r^* = 0.95$; Definition 1; see Tables 2 and 3 and Fig. 9a,c). The major difference is in the Weddell Sea, since the previously-discussed control anomaly in years 30-60 influences the Monte Carlo experiments, but not the Scenario A experiment under Definition 1. The ensemble mean of the MC simulations under Definition 2 (explained variance: 67%; Fig. 9b) shows a larger signal in the Arctic and reduced variance in the Antarctic relative to Definition 1. As for Definition 1, averaging the MC ensemble yields a signal which is even more highly correlated with the EOF 1 pattern of SZA ($r = 0.92$, $r^* = 0.98$; see Tables 2 and 3). These results, together with the high correlation between EOF 1 of the MC ensemble means under both definitions ($r = 0.75$, $r^* = 0.92$), show that ensemble averaging is a useful tool to isolate the climate change signal in short and noisy samples.

correlation between Def1 and Def2	MC00	MC30	MC60	MC90	MC mean	SZA
MC00	**0.28**	0.16	0.62	0.64	0.76	0.84
MC30	*0.61*	**0.29**	0.31	0.18	0.59	0.39
MC60	*0.45*	*0.91*	**0.88**	0.84	0.87	0.87
MC90	*0.53*	*0.93*	*0.96*	**0.92**	0.83	0.84
MC mean	*0.76*	*0.96*	*0.91*	*0.90*	**0.92**	0.95
SZA	*0.67*	*0.96*	*0.93*	*0.96*	0.98	**0.90**

Table 3: Between-integration pattern correlations for EOF 1 of the individual members of the ensemble of MC experiments and the mean of the ensemble. All correlations are computed without removal of the spatial mean component (r^*). Results are for Definition 1 (upper triangle of matrix) and Definition 2 (lower triangle of matrix and italics) of the signal. The diagonal elements of the matrix (bold) give the correlation of the EOF 1 pattern of the same experiment under the two definitions.

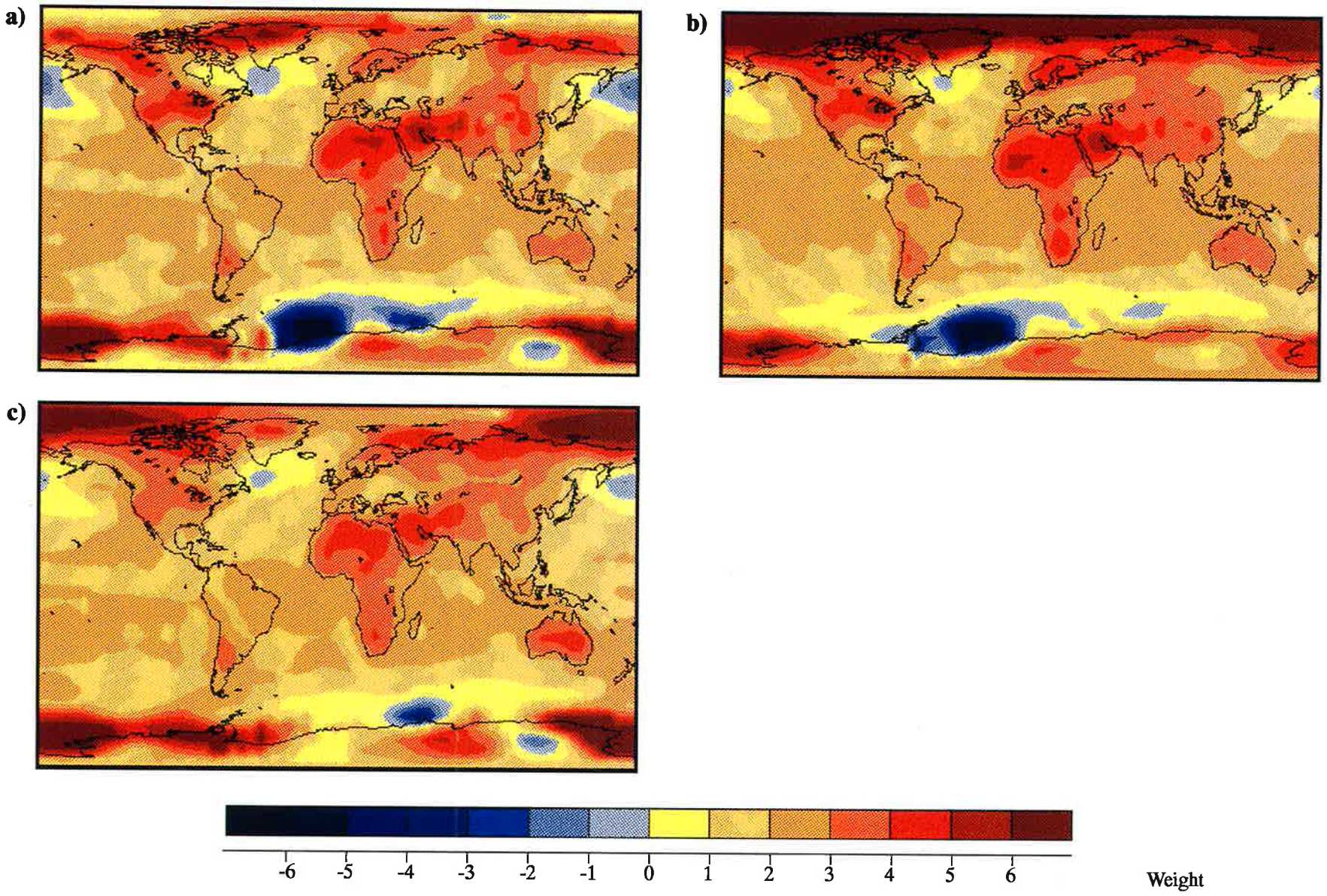

Figure 9. The first EOF [*10^2] of the near surface temperature change of the MC ensemble (Definition 1: a), Definition 2: b), and c) of the 100 year scenario A experiment after Cubasch et al (1992).

3.2.3 Sea Ice

The previous sections showed that temperature changes are of largest amplitude in the polar regions largely due to changes in the sea-ice coverage and thickness. In order to better understand the results of the MC simulations, it is useful to examine whether the coupled model simulates realistic changes in the distribution and thickness of sea-ice in the control run.

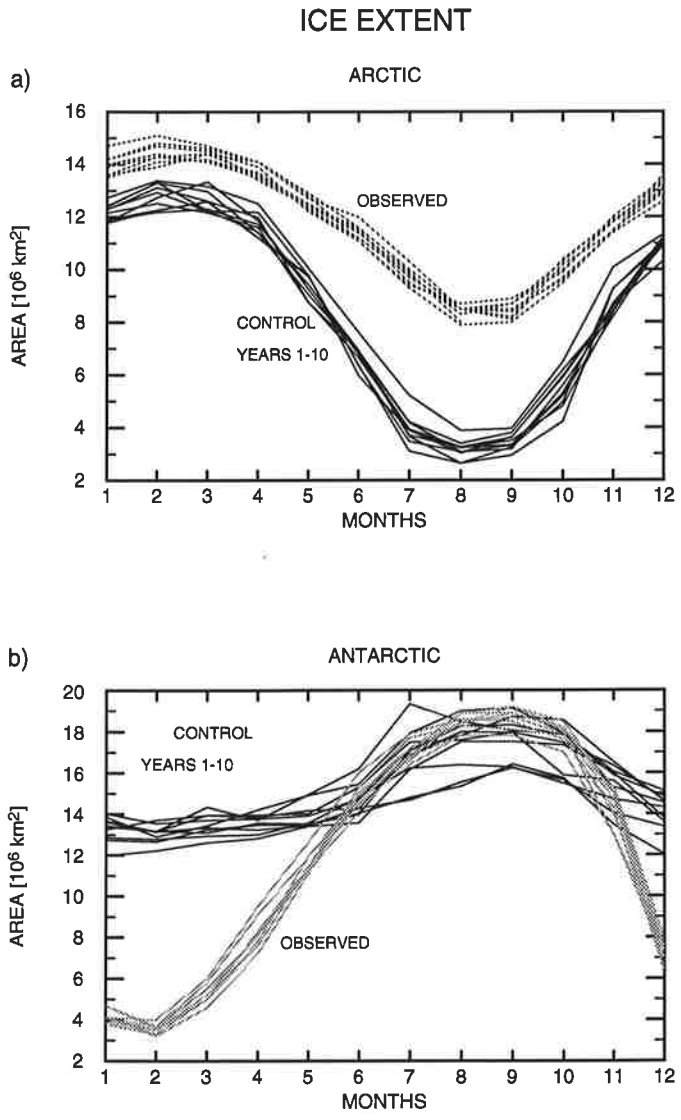

Figure 10. The annual cycle of the ice extent of the first 10 years of the control simulation and observed after Gloerson and Campbell (1988). a): Arctic; b): Antarctic.

The interannual fluctuations in ice extent of the control simulation (Fig. 10) are within the observed range of variability (Zwally et al., 1983; Parkinson, 1991, 1992), though somewhat overestimated in the Southern Ocean. The most crucial variable for evaluating the skill of sea-ice simulations, however, is the areal sea-ice thickness distribution. Its integrated product is the ice volume. In the control simulation, sea ice requires about 60 years in the northern hemisphere to equilibrate from an initial volume of 11 . 10^3 km^3 to a mean ice volume of about 40 . 10^3 km^3 (Fig. 11a). In the southern hemisphere, the same simulation yields an ice volume of up to 65 . 10^3 km^3 after about 70 years starting from an initial mean ice volume of 25 . 10^3 km^3 (Fig. 11b). For comparison, the present day annual mean sea-ice volume is about 20 . 10^3 km^3 in the northern hemisphere (see e.g. Loewe, 1987) and approximately 10 to 16 . 10^3 km^3 in the southern hemisphere (Parkinson and Bindschadler, 1984; Stössel et al., 1990).

In the MC simulations, the ice volume in the northern hemisphere generally decreases if Definition 2 is applied. As the ice extent is not significantly changed, the ice thickness decreases. In the southern hemisphere the ice volume increases in the first and third experiment (MC00, MC60) after application of Definition 2, but decreases for the other two experiments. The ice extent remains stable. The only large change is caused by a sudden decrease of ice coverage in the control experiment due to a melting of the ice in the Weddell sea, an event which is not simulated in any of the MC simulations. This decrease in the ice coverage in the control simulation is more than twice as large as the change in any of the MC simulations.

The simulations yields ice-volume increases of more than twice to up to four times the initial values. Similar discrepancies are obtained when compared with present day ice volumes. This unrealistic behavior in the simulations make an evaluation of the results, especially those of the climate change experiments, in sea ice covered regions rather difficult.

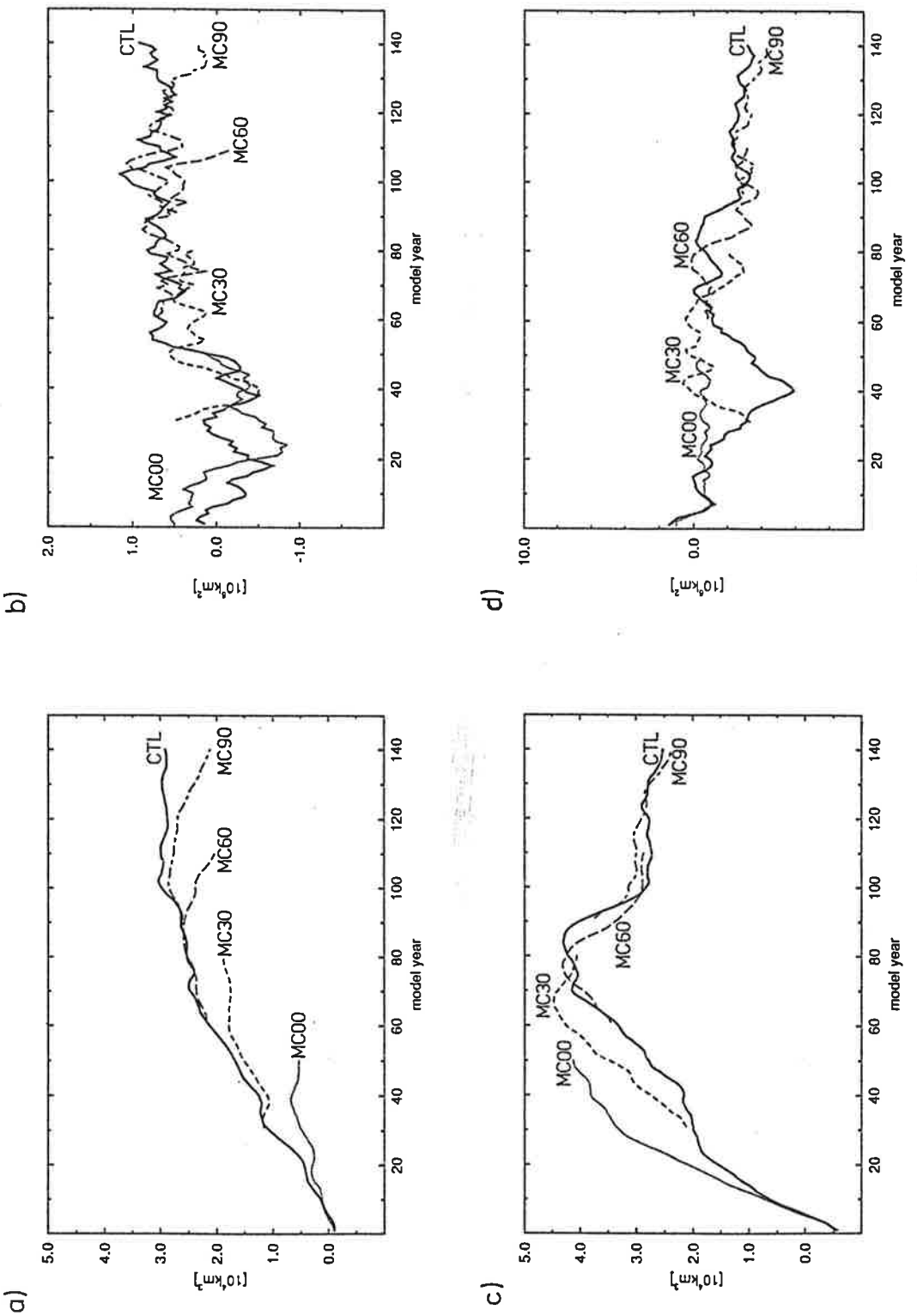

Figure 11. The time evolution of the change of the ice volume in the northern (a) and southern (c) hemisphere as well as the time evolution of the change of the maximum ice extend in the northern (b) and southern (d) hemisphere relative to the first decade of the control experiment.

The large ice volume in the Southern Ocean is caused by isolated grid points within the ice pack reaching highly overestimated thicknesses of 10 m and more. This leads to a severe underestimation of the seasonal cycle of the ice extent as compared to observations obtained by remote sensing (Gloersen and Campbell, 1988; Fig. 10b). While in the winter in the southern hemisphere the simulated ice extent coincides with observations, the ice fails to melt away in the South summer due to the large ice thickness. The summer ice extent is therefore reduced by only 23% compared to winter, while in the observations reductions of up to 80% are quite common. In the MC simulations, the ice-melt in summer is increased, while the winter ice extent remains the same. The seasonal cycle is therefore enhanced under climate change conditions.

In the Arctic Ocean, on the other hand, the seasonal cycles of ice extent are overestimated in the beginning of the control integration, which is reflected by a summer ice extent of about one third of the observed value (Fig. 10a). The climate change conditions of the MC simulations do not significantly alter the seasonal cycle in the northern hemisphere.

The increase of ice volume in the Arctic during the integration is primarily caused by local increases of ice thicknesses, which eventually reaches values, which locally prevent the ice from melting in summer. Since these increases are constrained to isolated gridpoints, the summer ice extent hardly increases during the integration (about $5 \cdot 10^6$ km^2 during years 91-100 of the control integration).

The reasons for the problems in the sea ice simulation seem to be related to the application of the flux correction and to the crude treatment of sea ice in the coupled simulations. Specifically, large heat fluxes may occur due to flux corrections in grid cells, where the uncoupled simulation did not reveal climatologically consistent sea-ice conditions or where the heat flux in the ocean varies strongly due to fluctuations in the upwelling. When

these flux corrections are continuously applied in a grid cell, where the sea-ice conditions or the upwelling rate has changed due to the coupling procedure, unrealistic accumulations are the consequence.

The present sea-ice formulation with over-simplified dynamics and thermodynamics, on the other hand, generally leads to higher sensitivities with respect to the ambient conditions, and therefore cannot compensate the unrealistic forcing. As the ice drift is essentially determined by the currents of the uppermost layer of the OGCM, this leads to severe underestimations of the ice drift in major parts of the divergent regions within the Antarctic ice pack, which is mostly wind driven (Stössel et al., 1990). As a results, the areal ice-thickness distribution (not shown) is far from representing the typical dynamically induced characteristics. Instead, the overestimated ice thicknesses are thermodynamically induced, being highly controlled by flux corrections of the order of 100 W/m^2.

Generally it has to be stated that the presently used sea ice component of the coupled model has only a limited capabililty to simulate the present day climate, similar to other models used in climate change experiments (Houghton et al, 1992). Predicted climate changes over regions with sea ice coverage should therefore be treated with caution.

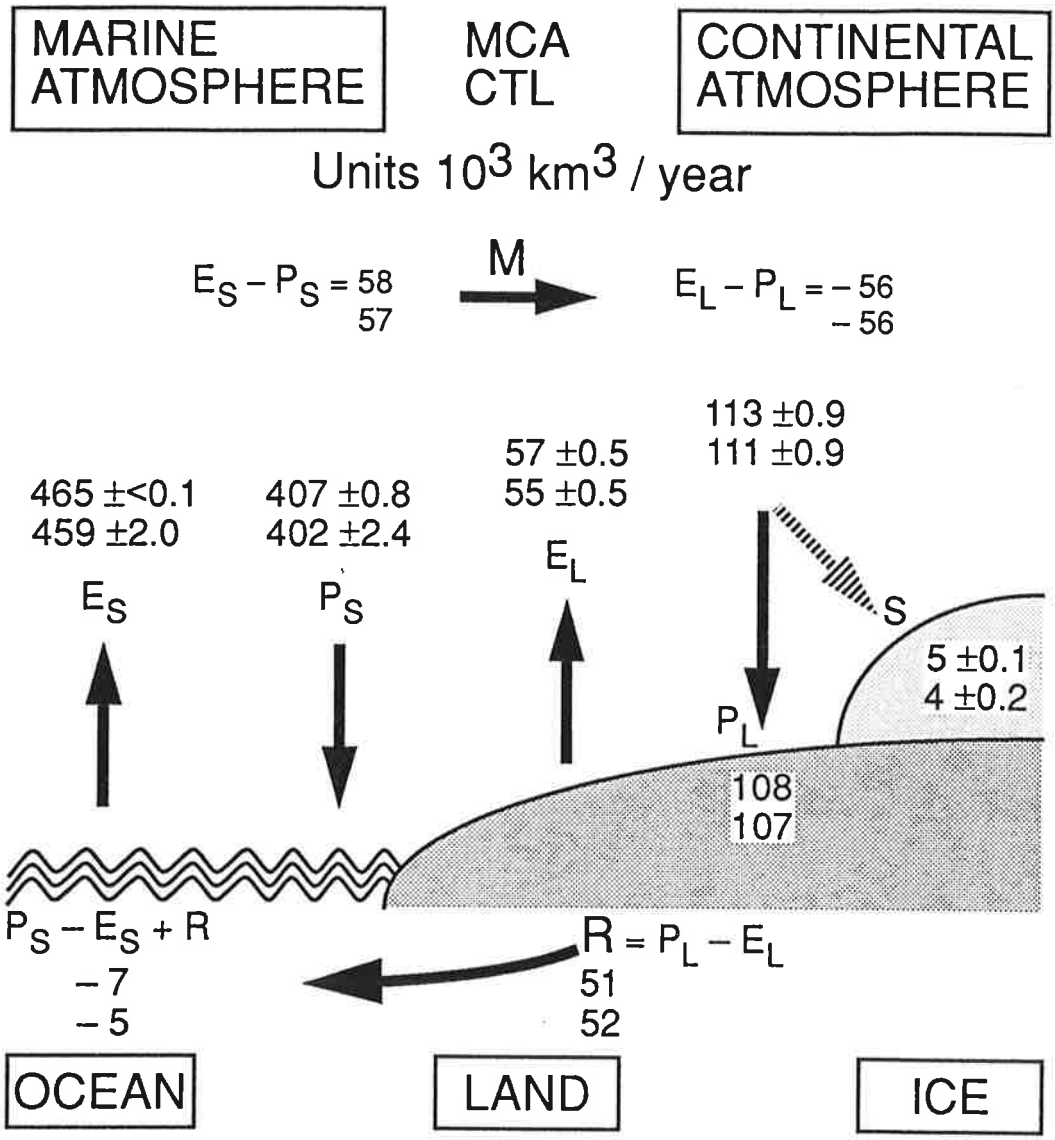

E_S, E_L	Evaporation	(sea, land)
P_S, P_L	Precipitation	(sea, land)
S	Snow deposition on land ice	
M	Moisture transport	
R	Runoff	

Figure 12. The hydrological cycle in the control experiment and in the ensemble of the climate change integrations.

3.2.4 Hydrological Cycle

The simulation of the global mean hydrological cycle of the control experiment is within the uncertainty range of the available observations (Baumgartner and Reichel, 1975).

Following Definition 1, the modelled hydrological cycle has generally increased by 2% after 50 years of simulation with the forcing of scenario A (Fig. 12) and is almost one order of magnitude larger than the standard deviation of the MC ensemble. About 25% more fresh water is deposited on the permanent ice. Together with increased evaporation, this leads to a net fresh water loss of 1000 km^3/year, which would result in a lowering of the sea-level by 30 cm within 100 years. The control simulation already has a high water deficit of about 120 cm within 100 years, as the snow which falls onto ice covered land areas is stored and cannot be recycled into the ocean, because this effect has not yet been parameterized. However, this does not influence the ocean circulation negatively, as this deficit in the mean is automatically compensated by the flux correction (Cubasch et al, 1992).

The change in the precipitation pattern shows very little spatial coherence, regardless of whether Definition 1 or Definition 2 is used. This noisy appearance makes it difficult to separate the climate change from the internal variability. The standard deviation of the MC simulations (Fig. 13) is as large as the signal. An univariate t-test consequently shows no region of significant precipitation change at the 95% level. The precipitation should therefore not be used for regional climate change studies. Nevertheless, the following statements about the regional distribution of precipitation change have been attempted (following Definition 1), because the IPCC reports explicitly mentions this quantity: There are indications that the rainfall increases in the mid-latitudes of the northern hemisphere in northern winter (Fig. 13b) and in the monsoon region in northern summer (Fig. 13a), similar to the findings in the IPCC report (Houghton et al, 1992).

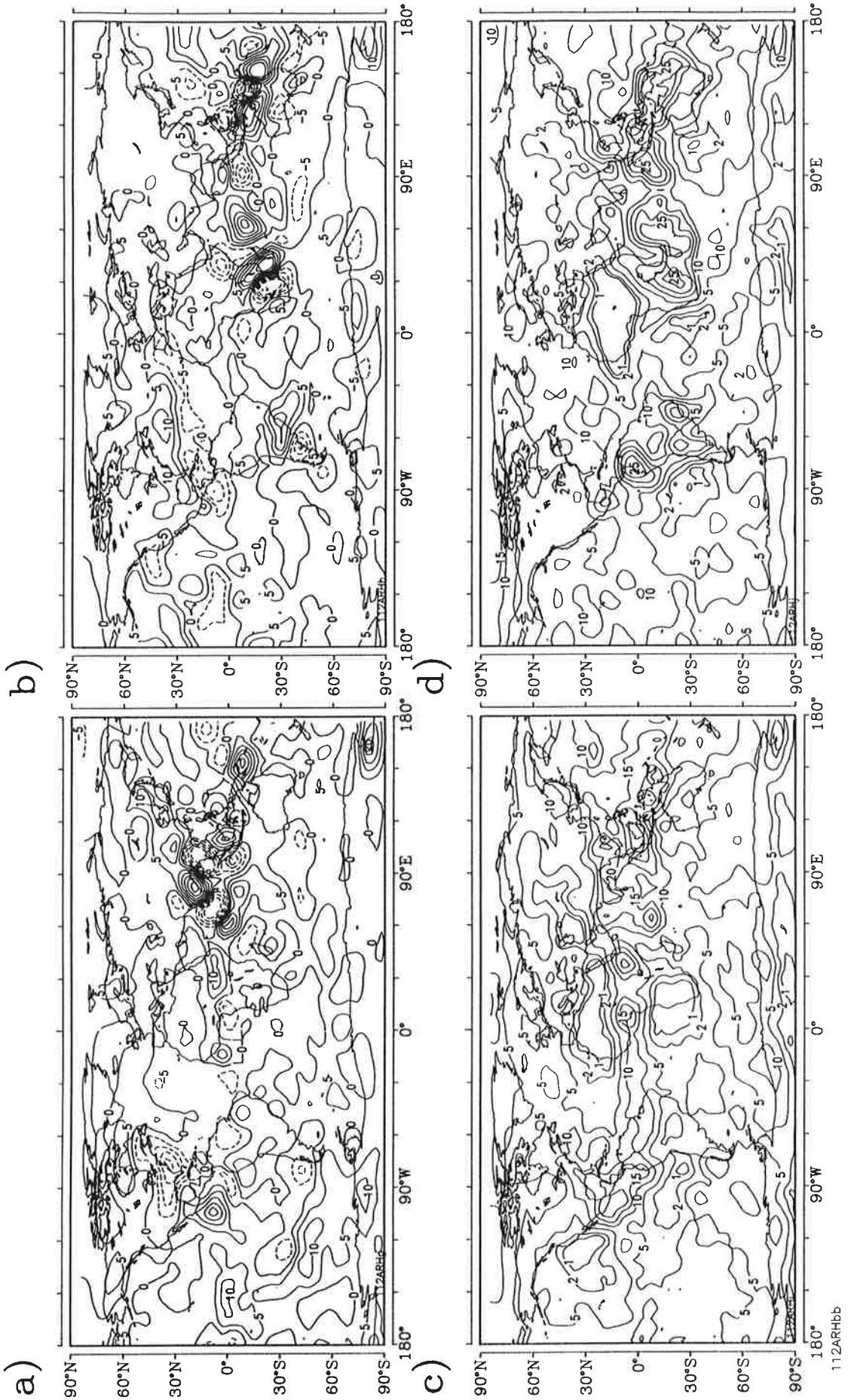

Figure 13. The distribution of the change in the ensemble averaged precipitation (Definition1) for the final decade of the MC integrations for the summer season (a) and the winter season (b) as well as the standard deviation of the precipitation change of the members of the ensemble to the mean in the summer season (c) and in the winter season (d).

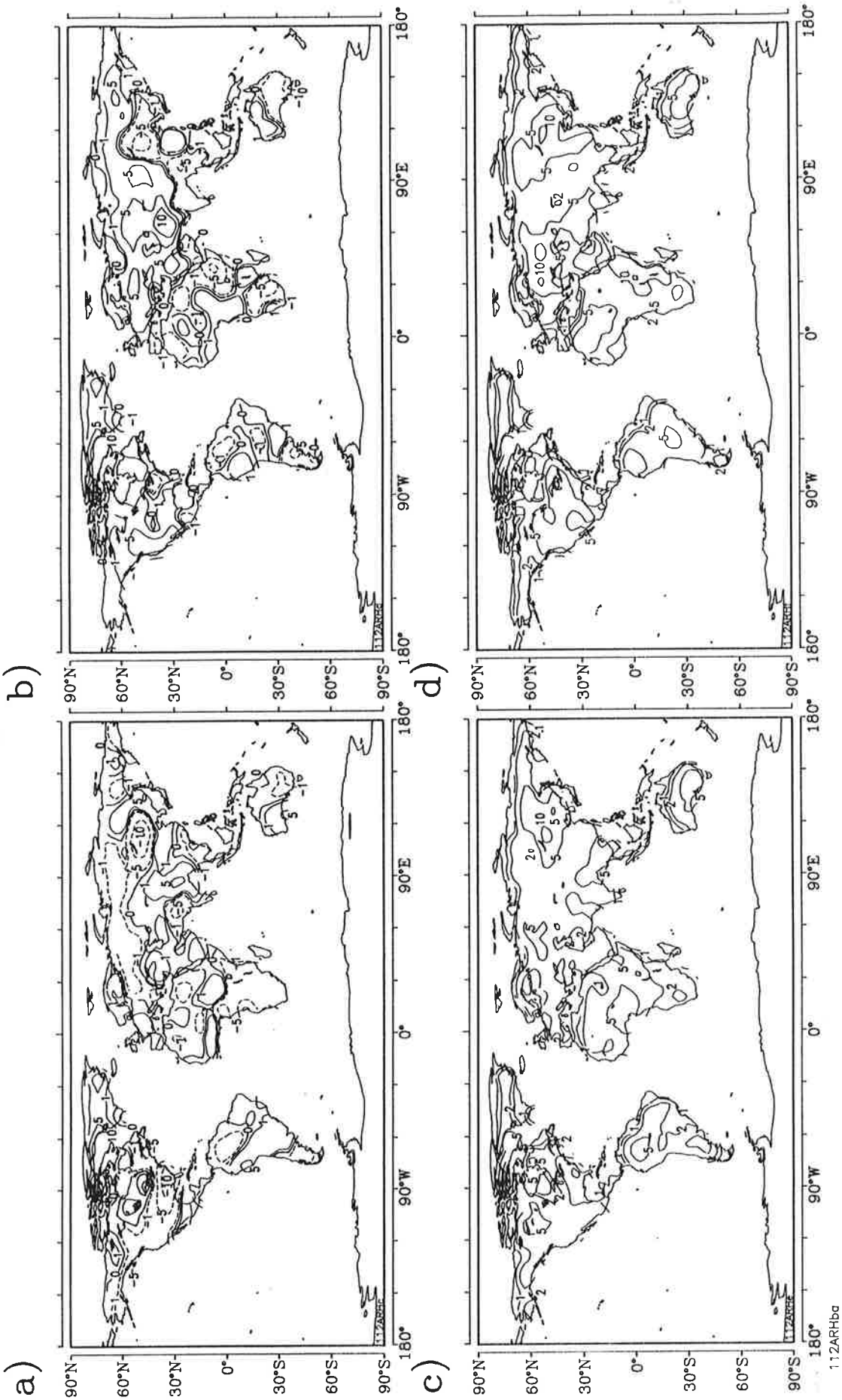

Figure 14. The distribution of the change in the ensemble averaged soil-moisture (Definition1) for the final decade of the MC integrations for the summer season (a) and the winter season (b) as well as the standard deviation of the soil-moisture change of the members of the ensemble to the mean in the summer season (c) and in the winter season (d).

Particularly the increased rainfall at the east coast of the US appears to be a stable feature in the northern winter season. In northern summer the north American continent experiences a decrease in precipitation. However, this decrease is strongly developed only in two of the four experiments. An increase of precipitation in the southern hemisphere storm-tracks, as suggested by IPCC (1992), cannot be identified as a stable feature.

The predicted climate change pattern for soil moisture is generally as noisy as for the precipitation. If Definition 1 is applied, the soil moisture increases over wide areas of the northern hemisphere in the northern winter (Fig. 14b). This seems to be a stable phenomenon of all the integrations. India experiences a decrease of soil moisture, while Australia experiences as many dry as moist events.

In the northern summer season the US, India and Africa south of the equator generally become drier (Fig. 14a) in agreement with the IPCC (1992) results, while the s signal over Australia and Europe varies strongly. It again must be stressed that because of the large between experiment standard deviation, no statistical significance can be attributed to any of the soil moisture change patterns (Fig. 14c, 14d) in an univariate t-test.

3.3 Sea Level Rise

The sea level changes presented in this section contain only the effects of thermal expansion and dynamic topography. The effect of glacier melting and the hydrological cycle are not included. The sea level rise has been calculated as the difference relative to the control run at the same year (Definition 2), as in Cubasch et al (1992), since the sea level in the control integration shows a drift of about 1.5 cm during the first 50 years before it seems to exhibit long periodic oscillations. Contrary to the behavior of the global mean temperature, the sea level rise after 50 years of integration time is almost identical in all four simulations (Fig. 15). The average sea level rise in the MC calculations is 4.2 cm within 50 years, with an RMS error in the order of 0.2 cm.

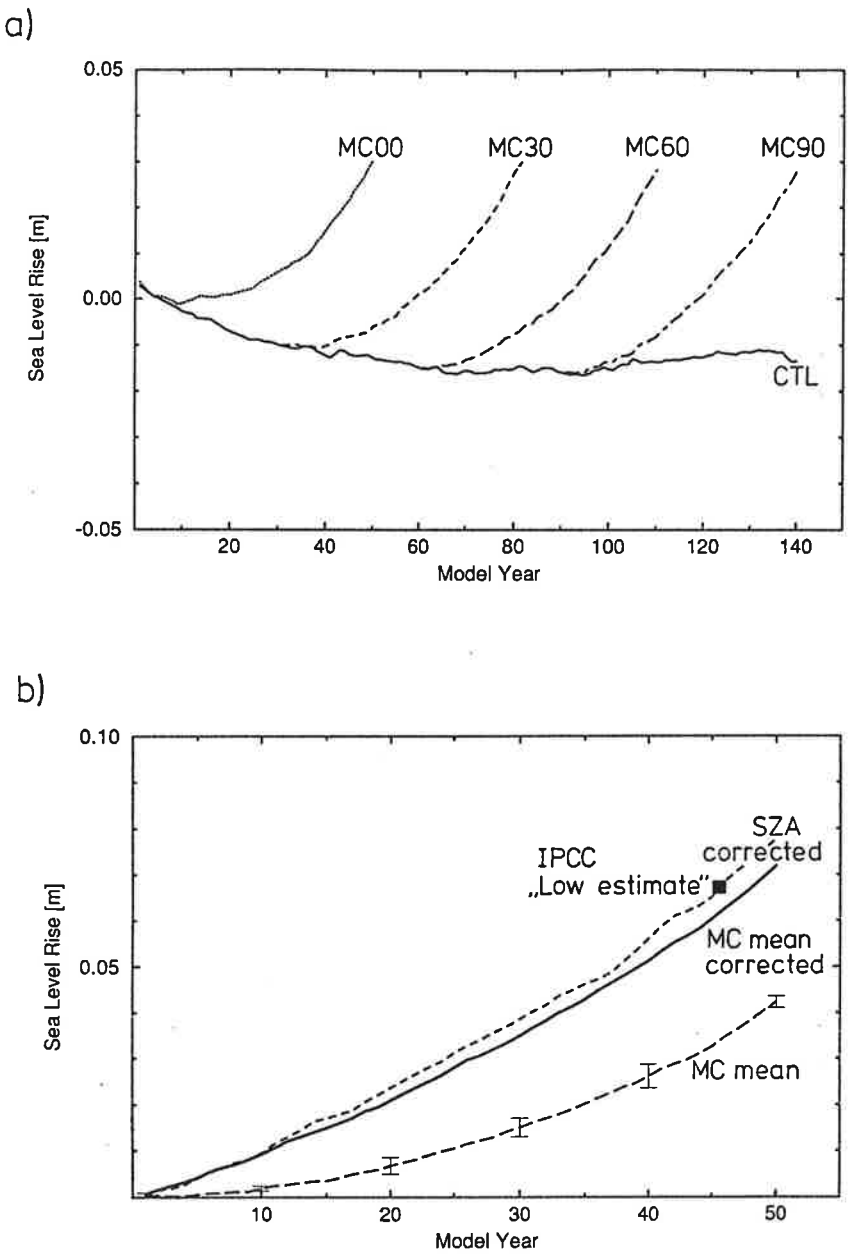

Figure 15. Time evolution of the global mean sea level change (cm) due to thermal expansion for the four "Monte-Carlo" Simulations and the control experiment (a); the time evolution of the global mean sea level change (cm) for the ensemble mean, the cold start corrected ensemble mean, the cold start corrected scenario A calculation after Cubasch et al (1992), the 95% significance limit for the uncorrected ensemble as well as the IPCC "low" estimate for the year 2035 after Houghton et al (1990) (b).

Following Hasselmann et al (1992), a correction for the "cold start" has been calculated from the ensemble mean sea level rise. It is in the order of 3 cm within 50 years and represents a substantial additional contribution to the sea level rise (Fig. 15b). The rate of corrected sea level rise falls well within the bracket quoted in the IPCC report (Houghton et al, 1992). It is, however, lower than the values obtained by a box diffusion model for the

"best" and even slightly below the "low" IPCC (Houghton et al, 1990) estimate. It is also slightly lower than the values obtained by Hasselmann et al (1992) for a single integration.The sea level rise during the first 50 years is to about 25% of the value after 100 years.

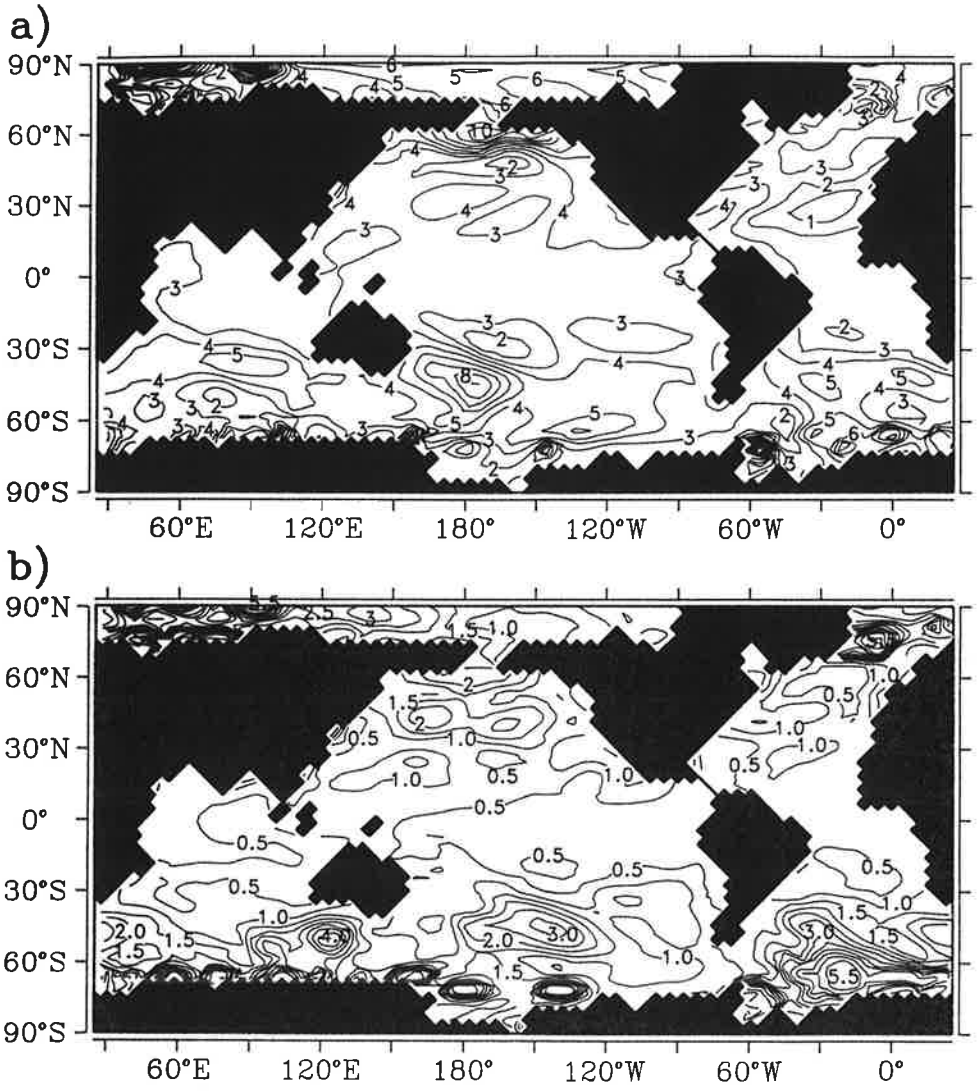

Figure 16. The horizontal distribution of the mean sealevel change of the ensemble mean for the last decade of the simulation (a) and the standard deviation of the members of the ensemble to the mean (b) after Definition 2 [unit: cm].

The horizontal pattern of sea level rise is comparatively stable (Fig. 16). The individual experiments show similar regions of increased sea level, particularly near the Bering Strait and at the northern edge at the Antarctic Circumpolar Current (ACC), probably due to a poleward shift of the ACC. The relatively small scale extreme values near the poles are

connected with the difficulties in the treatment of the sea ice. The regional differences in sea level rise have approximately the same size as the global mean signal. A similar result has been found by Mikolajewicz et al (1990). In the ensemble mean the sea level rise pattern closely resembles the pattern obtained after 100 years of integration time, but with much reduced amplitude.

The sea level change exhibits a large between integration variability only around the ACC and in regions with sea ice. Therefore, an univariate t-test (95%) reveals areas of significant sea-level rise due to thermal expansion in the Indian Ocean, the northern edge of the ACC as well as the North and Central Pacific, while in the Atlantic and the central and southern ACC only limited regions can be labelled significant.

4.0 Summary

Generally the MC experiments confirm the findings of the 100 year integration made with the same model (Cubasch et al, 1992; Santer et al, 1992). But, even with such a small sample, the MC approach provides additional information not available from a single integration:

The method enables the estimation of not only of the mean response, but also of the variability around the mean signal and about the regional distribution of the areas with the largest uncertainty. This uncertainty might be caused by internal variability or by drift of the system. Individual members of the ensemble show quite different climate change patterns and amplitudes, so that a single integration, at least over a time period of 50 years, might give misleading results. After 100 years of simulation time the experiment by Cubasch et al (1992) gives a climate change prediction whose pattern is close to the mean of the MC ensemble. The climate change signal can be more clearly isolated with the MC method than would have been possible from a single short integration.

In a global mean, the climate change signal for near surface temperature, the hydrological cycle and sea level significantly exceed the variability among the members of the ensemble. Due to the high internal variability of the modelled climate system, the estimated detection time of the global mean temperature change signal is uncertain by at least 1 decade.

Due to the short integration time of only 50 years the temperature change pattern of the individual members of the ensemble show a large variability. This is consistent with the studies by Cubasch et al (1992) and Santer et al (1992), where it was found that a stable climate change signal could be defined only in the second half of a single 100 year integration.

While the local temperature and sea level change are at least in some regions significant in the ensemble mean, it is not possible to identify a characteristic climate change pattern of the precipitation and the soil moisture fields, because their climate change pattern are spatially noisy and are characterized by large variability between the individual integrations. This agrees with results obtained by Santer et al, 1992, where changes in precipitation were difficult to separate from the coupled model's inherent climate variability and/or drift.

The seasonal patterns of the ensemble mean temperature change agree reasonably well with the results published in the recent IPCC report (Houghton et al, 1992). An increase in precipitation in the storm tracks of the southern hemisphere, as suggested in the same IPCC report, could not be verified.

There is little difference in the predicted sea-level rise due to thermal expansion between the experiments in the global mean, but the simulated values are still slightly lower than the IPCC estimate, even when corrected for the cold start. The cold start contributes substantially to the sea level rise in the time period considered. After 50 years integration time

more than a third of the contribution to the sea level rise is estimated to arise from the cold start error.

The results of climate change experiments are generally very sensitive to the actual definition of a climate change. The results can vary considerable, depending, on what assumptions regarding the cause of the changes in the state of the control experiment are made, i. e. whether they are considered as internal fluctuations or drifts, and what definition is therefore used to calculate the climate change. In our study, a cooling or a warming can be obtained in the Arctic for the same experiment, just by applying different definitions for the climate change. A larger ensemble might reduce uncertainties and clarify whether an unusual response has been obtained by chance, or represents an more frequently emerging state. Furthermore, in order to gain more reliable statements about climate change from globally coupled ocean-atmosphere models in the high latitudes, it seems to be necessary to incorporate a more sophisticated formulation of the sea-ice component and to reduce the size of the flux correction.

The MC simulations complement the longer 100 year scenario A experiment. While the long experiment was necessary to establish a stable climate change pattern for the near surface temperature, the MC simulations give an estimate of both, the climate change pattern and its uncertainties in the next 50 years.

Acknowledgments

We wish to thank K. Hasselmann, L. Bengtsson, E. Roeckner, H. Grassl and G. Boer for their helpful discussions and their support in the scientific aspects of the paper. P. Lenzen and R. Gaedtke provided for the data handling. N. Noreiks and M. Grunert drew the diagrams. The research has been supported by the German Ministery for Research and Technology (BMFT), the Max-Planck-Gesellschaft, the Freie und Hansestadt Hamburg and the EC Environmental program. The authors are grateful to the staff of the DKRZ for their excellent technical support

References

Bakan, S, Chlond A, Cubasch U, Feichter J, Graf H F, Grassl H, Hasselmann K, Kirchner I, Latif M, Roeckner E, Sausen R, Schlese U, Schriever D, Schult I, Schumann U, Sielmann F, Welke W (1991) Climate response to smoke from the burning oil wells in Kuwait. Nature 351: 367-371

Baumgartner A and Reichel E (1975) The world water balance: mean annual global continental and maritime precipitation, evaporation and runoff. R. Oldenbourg, München-Wien, 179 pp

Brankovic C, Palmer T N, Molteni F, Tibaldi S and Cubasch U (1990) Extended range predictions with the ECMWF models: time lagged ensemble forecasting. Quart. J. Roy. Met. Soc. 116, 835-866

Cubasch U, Hasselmann K, Hoeck H, Maier-Reimer E, Mikolajewicz U., Santer B D and Sausen R (1992) Time-dependent greenhouse warming computations with a coupled ocean-atmosphere model. 'Climate Dynamics', in print

Fichefet T and Tricot C (1992) Influence of the starting date of model integration on projections of greenhouse-gas-induced climatic change. Geophysical Res. Letters, in press.

Gloersen P and Campbell W J (1988) Variations in the arctic, antarctic, and global sea ice covers during 1978 to 1987 as observed with the Nimbus 7 scanning multichannel microwave radiometer. J. Geophys. Res. 93: 10666-10674

Hansen J, Fung I, Lacis A, Rind D, Lebedeff S, Ruedy R, Russell G and Stone P (1988) Global climate changes as forecast by GISS three-dimensional model. J. Geophys. Res. 93: 9341-9364

Hasselmann K, Sausen R, Maier-Reimer E and Voss R (1992) On the cold start problem with coupled ocean-atmosphere models. MPI Report No. 83, MPI für Meteorologie, Hamburg, FRG

Houghton J T, Jenkins G J and Ephraums J J (eds.) (1990) Climate change. The IPCC scientific assessment. Cambridge University Press, Cambridge, 364 pp

Houghton J T, Callander B A and Varney S K (eds.) (1992) Climate Change 1992. The supplementary report to the IPCC scientific assessment. Cambridge University Press, Cambridge, 200 pp

Lorenz E N (1991) Chaos, spontaneous climatic variations and detection of the greenhouse effect. In: greenhouse gas induced climatic change: a critical appraisal of simulations and observations. M. Schlesinger (ed); Elsevier, Amsterdam, 615 pp

Loewe P (1987) Sea ice simulations performed with forcing fields specified from a GCM.Techn. Rep. 6/87, Cold Regions Research Lab. 72, Hanover, New Hampshire 03755, USA

Manabe S, Spelman M J and Stouffer R J (1992) Transient responses of a coupled ocean-atmosphere model for gradual changes of atmospheric CO_2. Part II: seasonal response. Journal of Climate 5: 105-126

Meehl G A, Washington W M and Karl T R (1992) Low-frequency variability and CO_2 transient climate change. Part I: time-averaged differences. Climate Dynamics, in press

Mikolajewicz U, Santer B D and Maier-Reimer E (1990) Ocean response to greenhouse warming. Nature 354: 589-593

Mikolajewicz U and Maier-Reimer E (1990) Internal secular variability in an ocean circulation model; Climate Dynamics 4: 145-156

Molteni F, Cubasch U and Tibaldi S (1988) 30- and 60-day forecast experiments with the ECMWF spectral models. In: Persistent meteo-oceanographic anomalies and teleconnections; C. Chargas and G. Puppi (eds.), Pontificiae Academiae Scientiarum Scripta Varia, MCMLXXXVIII

Mysak L A and Manak D K (1989) Arctic sea-ice extent and anomalies, 1953-1984; Atmosphere-Ocean 27: 376-406

Parkinson C A and Bindschadler R A (1984) Response of antarctic sea ice to uniform atmospheric temperature increases. in: Climate Processes and Climate Sensitivity, Geophysical Monograph 29, Maurice Ewing Volume 5, AGU

Parkinson C A and Cavalieri D J (1989) Arctic sea ice 1973-1987: seasonal, regional and interannual variability. J. Geophys. Res. 94: 14 499-14 523

Parkinson C A (1991) Interannual variability of the spatial distribution of sea ice in the North pole region. J. Geophys. Res. 96: 4791-4801

Parkinson C A (1992) Interannual variability of monthly southern ocean sea ice distributions. J. Geophys. Res. 97: 5349-5363

Santer B D, Brüggemann W, Cubasch U, Hasselmann K, Höck H , Maier-Reimer E and Mikolajewicz U (1992) Signal-to-noise analysis of time-dependent greenhouse warming experiments. Part 1. Pattern Analysis. submitted to "Climate Dynamic'

Stössel A, Lemke P and Owens W B (1990) Coupled sea ice-mixed layer simulations for the southern ocean. J. Geophys. Res. 95: 9539-9555

Stössel A (1992) Simulations to different atmospheric forcing algorithms. Tellus, in press.

Stössel A and Claussen M (1993) A new atmospheric surface-layer scheme for a large scale sea-ice model. MPI Technical Report, MPI für Meteorologie, Hamburg, FRG

Wigley T M L. and Santer B D (1990) Statistical comparison of spatial fields in model validation, perturbation and predictability experiments. J. Geophys. Res. 95: 851-865

Zwally H J, Comiso J C, Parkinson C L, Carsey F D, Campbell W J and Gloersen P (1983) Antarctic sea ice 1973-1976: satellite passive-microwave observations, NASA Spec. Publ., SP - 459, 1-206